



SEMIANALYTIC SENSITIVITY ESTIMATES FOR OUT-OF-BANK GRAVITATIONAL-WAVE SIGNALS

ADITYA VIJAYKUMAR ¹ AND REED ESSICK ^{1,2,3}

¹Canadian Institute for Theoretical Astrophysics, University of Toronto, 60 St George St, Toronto, ON M5S 3H8, Canada

²Department of Physics, University of Toronto, 60 St. George Street, Toronto, ON M5S 1A7 and

³David A. Dunlap Department of Astronomy, University of Toronto, 50 St. George Street, Toronto, ON M5S 3H4

Version June 15, 2026

ABSTRACT

Estimating the sensitivity of gravitational-wave searches is important for a wide variety of scientific applications spanning astrophysics and fundamental physics. In this work, we develop a fast semianalytic approximation for estimating matched-filter search sensitivity to physical effects not explicitly modeled in the template bank. This approximation utilizes fitting factors, i.e., the maximum overlap of a candidate signal over the search bank. As illustrations, we compare our estimates to the actual performance of searches against spinning binary neutron stars, and evaluate search sensitivity to compact binaries possessing orbital eccentricity or deviations from general relativity. Our work thus paves the way for fast sensitivity estimates for a variety of applications, including unmodeled effects in template banks such as deviations from general relativity, environmental effects, gravitational lensing, and waveform/calibration systematics.

1. INTRODUCTION

One distinctive feature of gravitational wave (GW) astronomy, as opposed to electromagnetic (EM) astronomy, is that selection effects can be estimated with high precision. This follows directly from the fact that the GW signal from compact binaries is completely specified by a fixed set of source parameters with very high precision, and the GW signal is not affected by matter along its propagation path, modulo gravitational lensing. This feature of GW signals is crucial for correcting selection biases and obtaining unbiased estimates of the underlying source population of merging binaries.

In practice, the selection function is estimated by building large sets of simulated GW signals embedded in realistic detector noise, referred to as *injections*. These injections are processed by search pipelines exactly as they would process real data; for each injection, detection statistics such as the signal-to-noise ratio (SNR), false alarm rate (FAR), and the probability of astrophysical origin (p_{astro}) are recorded (The LIGO Scientific Collaboration et al. 2026a; A. H. Nitz et al. 2023; A. K. Mehta et al. 2025). A realistic injection set for current catalogs (The LIGO Scientific Collaboration et al. 2026b, 2025a) typically contains $\sim 10^6$ injections (R. Essick et al. 2025; LIGO Scientific Collaboration et al. 2025), making this process significantly intensive in terms of computational- and person-power. The required number of injections also grows approximately linearly with catalog size (R. Essick & W. Farr 2022). Therefore, while in-principle straightforward, calculating the selection function is non-trivial in practice. These difficulties compound if selection effects need to be estimated for a wide variety of applications, e.g., for eccentric sources, for signals motivated by modified gravity theories, etc. Approaches that either learn the selection function from injection sets (D. Gerosa et al. 2020; C. Talbot & E. Thrane 2020; T. A. Callister et al. 2024) or calibrate simple-to-evaluate expression to them (M. Mould et al. 2024; A. Lorenzo-Medina & T. Dent 2025) also suffer from related issues because they

are predicated on the existence of large injection sets for training data.

Thus, methods for making this process faster are desirable. Semianalytic approaches (L. S. Finn & D. F. Chernoff 1993; R. Essick 2023) are one solution. The fundamental idea behind this proposal is that the observed SNR is distributed around the optimal SNR following a non-central χ distribution with $2N_{\text{det}}$ degrees of freedom, where N_{det} is the total number of detectors in the network. The spread around the optimal SNR is driven by fluctuations in the detector noise. R. Essick (2023) showed that a semianalytic SNR threshold of ≈ 10 reproduces the detected distribution of the O3 injection set under a FAR $< 1 \text{ yr}^{-1}$ cutoff. Similar ideas have been explored in other works (D. Wysocki et al. 2019; D. Gerosa & M. Bellotti 2024).

While this method is effective, it suffers from a few drawbacks. First, current matched-filter searches used by the LIGO-Virgo-KAGRA (LVK) Collaboration (LIGO Scientific Collaboration et al. 2015; F. Acernese et al. 2015; T. Akutsu et al. 2021) do not include the effect of eccentricity or spin-precession in their template banks. This means that traditional semianalytic estimates, which assume all the relevant physics is included within the template bank, only provide an upper bound on sensitivity to such effects. Secondly, the method also does not account for the finite spacing of template banks and assumes that the template bank is infinitely dense in all regions of the signal parameter space. As evidenced by choices in, e.g., S. Sakon et al. (2024) and discussed in §3, real template banks are discrete and might lack coverage in some regions of the source parameter space. As an example, consider an extreme case where a signal has zero overlap with every template in a bank. Because the semianalytic prescription is independent of template bank structure and coverage, it would categorize such a signal as detectable based solely on its true SNR. In reality, however, the search sensitivity is identically zero. Additionally, while traditional semianalytic estimates might be able to mimic the detection statistic, they cannot provide other

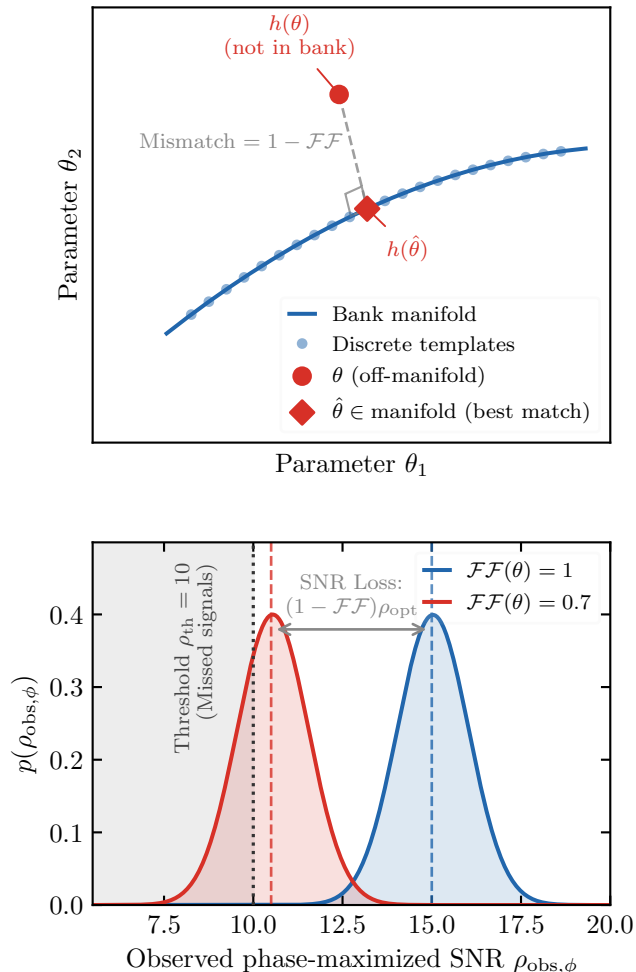


FIG. 1.— *Illustration of our method.* The top panel shows the template bank manifold in the blue solid line, with the discreteness of the bank denoted by blue points. A candidate signal described by $h(\theta)$ and optimal SNR $\rho_{\text{opt}}(\theta)$ outside the bank has a best match template $h(\hat{\theta})$ in the bank, incurring a mismatch $1 - \mathcal{FF}(\theta)$ in the process. Thus, in the bottom panel, this translates to a reduced non-centrality parameter $\mathcal{FF}(\theta)\rho_{\text{opt}}$ for the distribution of the observed phase-maximized SNR $\rho_{\text{obs},\phi}$, reducing the detectability of the signal. In this setup, $\mathcal{FF}(\theta) = 0.7$ and 29% signals are missed, whereas if $\mathcal{FF}(\theta) = 1$ only $2.3 \times 10^{-5}\%$ signals are missed.

information that searches provide, e.g., the best match template parameters for each injection.

In this work, we develop a framework for semianalytic sensitivity estimates that addresses these issues. Instead of assuming that a signal always has a closely matching template in the bank, we explicitly maximize the overlap of a candidate signal across the finite template bank before projecting it onto a detector network and incorporating the effects of noise. We demonstrate that our method reproduces a range of results reported in the literature. Furthermore, thanks to a GPU-accelerated maximization procedure, our technique is highly efficient and can produce realistic sensitivity estimates within just a few hours.

This paper is structured as follows. In §2, we lay out the mathematical framework underlying our method and

also detail various analysis settings and choices. In §3, we concentrate on three different applications: gaps and discreteness in existing template banks (§3.1), missing physics, like eccentricity, that is known but not included in the search manifold (§3.2), and missing physics that is unknown, like deviations from general relativity, and is therefore also not included in the search manifold (§3.3). We discuss other potential avenues for applications in §4 along with caveats and possible future improvements.

2. METHODS

2.1. Nomenclature

We model GW data in the frequency-domain $d(f)$ as

$$d(f) = h(f; \theta) + n(f), \quad (1)$$

where $h(f; \theta)$ represents the GW signal characterized by the parameters θ and $n(f)$ is additive, zero-mean, stationary Gaussian noise with one-sided power spectral density (PSD) denoted by $S_n(f)$. We define the noise-weighted inner product in the frequency domain as

$$\langle a|b \rangle = 4 \int_{f_{\text{low}}}^{f_{\text{high}}} \frac{a(f) b^*(f)}{S_n(f)} df, \quad (2)$$

where $b^*(f)$ is the complex conjugate of $b(f)$. Note that $\langle a|b \rangle$ is, in general, complex.

To identify potential signals, we filter the data against a template bank $\{h(\theta_T)\}$. By maximizing the stationary Gaussian likelihood with respect to the signal's amplitude, we can derive the matched-filter response of the data against a single template $h(\theta_T)$

$$\hat{\rho}(\theta_T) = \frac{\langle d|h(\theta_T) \rangle}{\rho_{\text{opt}}(\theta_T)}, \quad (3)$$

where $\rho_{\text{opt}}(\theta_T) = \sqrt{\langle h(\theta_T)|h(\theta_T) \rangle}$ is the optimal SNR of the template. Writing $\hat{\rho} = \hat{\rho}_R + i\hat{\rho}_I$, the real and imaginary parts are independent Gaussian random variables with unit variance. If the data contains a signal described by θ , then the expected values of the real and imaginary filter responses are

$$\mathbb{E}[\hat{\rho}_R] = \mathfrak{M}(\theta_T; \theta) \rho_{\text{opt}}(\theta) \cos \Delta\phi, \quad (4)$$

$$\mathbb{E}[\hat{\rho}_I] = \mathfrak{M}(\theta_T; \theta) \rho_{\text{opt}}(\theta) \sin \Delta\phi, \quad (5)$$

where

$$\mathfrak{M}(\theta_T; \theta) = \frac{|\langle h(\theta)|h(\theta_T) \rangle|}{\rho_{\text{opt}}(\theta_T) \rho_{\text{opt}}(\theta)} \quad (6)$$

is the match between the signal and template and $\Delta\phi$ is their relative phase offset. For compact binary coalescences (CBCs), $\Delta\phi$ could correspond to the orbital phase at coalescence. The phase-maximized filter response is then

$$\hat{\rho}_\phi(\theta_T; \theta) = \sqrt{\hat{\rho}_R^2(\theta_T; \theta) + \hat{\rho}_I^2(\theta_T; \theta)}. \quad (7)$$

One can show that $\hat{\rho}_\phi$ follows a non-central χ distribution with two degrees of freedom and non-centrality parameter

$$\lambda = \mathfrak{M}(\theta_T; \theta) \rho_{\text{opt}}(\theta). \quad (8)$$

Another quantity that is useful to calculate is the *fitting factor* (T. A. Apostolatos 1995), which is the match in Equation (6) maximized over the template bank

$$\mathcal{FF}(\theta) = \max_{\theta_T \in \text{bank}} \mathfrak{M}(\theta_T; \theta). \quad (9)$$

By definition, $0 \leq \mathcal{F}\mathcal{F}(\theta) \leq 1$. The equality $\mathcal{F}\mathcal{F}(\theta) = 1$ is satisfied when the best-matching template corresponds to the true signal.

In a network of N_{det} detectors, the network phase-maximized filter response is obtained by summing the individual detector responses in quadrature (i.e., maximizing over $\Delta\phi$ separately in each detector)

$$\hat{\rho}_{\phi}^{\text{net}}(\theta_T; \theta) = \sqrt{\sum_{i=1}^{N_{\text{det}}} [\hat{\rho}_{\phi}^i(\theta_T; \theta)]^2}. \quad (10)$$

$\hat{\rho}_{\phi}^{\text{net}}(\theta_T)$ is non-central χ distributed with $2N_{\text{det}}$ degrees of freedom and non-centrality parameter

$$\lambda^{\text{net}} = \sqrt{\sum_i^{N_{\text{det}}} [\mathfrak{M}^i \rho_{\text{opt}}^i]^2} \quad (11)$$

Importantly, the optimal SNR (ρ_{opt}^i), match (\mathfrak{M}^i), and fitting factor ($\mathcal{F}\mathcal{F}^i$) can be different in each detector because the PSDs can be different in each detector.

Searches often maximize the network response over the template bank, and we define

$$\hat{\rho}_{\text{obs},\phi}^{\text{net}}(\theta) = \max_{\theta_T \in \text{bank}} \{ \hat{\rho}_{\phi}^{\text{net}}(\theta_T; \theta) \}. \quad (12)$$

2.2. Approximating search behavior

In most matched-filter searches, the incoming data are filtered against a template bank and $\hat{\rho}_{\text{obs},\phi}^{\text{net}}$ from Eq. (12) is reported as one detection statistic. However, one can attempt to approximate $\hat{\rho}_{\text{obs},\phi}^{\text{net}}$ in a semianalytic fashion following the distribution of the matched-filter responses from §2.1. In particular, one reasonable approximation could be $\hat{\rho}_{\phi}(\theta_T; \theta) \approx \hat{\rho}_{\phi}(\theta; \theta)$, in which case

$$\hat{\rho}_{\text{obs},\phi}^{\text{net}}(\theta) \approx \hat{\rho}_{\phi}^{\text{net}}(\theta; \theta) = \sqrt{\sum_{i=1}^{N_{\text{det}}} [\hat{\rho}_{\phi}^i(\theta; \theta)]^2}. \quad (13)$$

Since the RHS of Equation (13) is the quadrature sum of $2N_{\text{det}}$ independent Gaussian random variables, $\hat{\rho}_{\text{obs},\phi}^{\text{net}}(\theta)$ also follows a non-central χ distribution with $2N_{\text{det}}$ degrees of freedom and non-centrality parameter

$$\lambda = \rho_{\text{opt}}^{\text{net}}(\theta) = \sqrt{\sum_i^{N_{\text{det}}} [\rho_{\text{opt}}^i(\theta)]^2}. \quad (14)$$

R. Essick (2023) shows that this approximation reproduces the behavior of searches under some choice of a threshold $\hat{\rho}_{\text{obs},\phi}^{\text{net}} \geq \rho_{\text{thr}}$. The effectiveness of this approximation is not surprising. Ideal search template banks are constructed to ensure $\mathcal{F}\mathcal{F}(\theta) \approx 1$ across the parameter space (B. J. Owen 1996); with this, the expectation value of the phase-maximized matched filter response approaches the optimal SNR.

However, when considering realistic, incomplete banks or unmodeled physical effects, we will generically have $\mathcal{F}\mathcal{F}(\theta) < 1$. To account for these effects when estimating sensitivity, it is then essential to include $\mathcal{F}\mathcal{F}(\theta)$ in our estimates—the recovered search SNRs will be reduced due to the $\mathcal{F}\mathcal{F}(\theta) < 1$ leading to a loss of detections,

thus impacting the sensitivity of GW searches. Thus, we approximate the expected value of the filter response as $\mathbb{E}[\hat{\rho}_R^i] \mathcal{F}\mathcal{F}^i(\theta)$. To reduce computational load, we further assume that the template yielding the maximum match and its corresponding $\mathcal{F}\mathcal{F}(\theta)$ are identical across all detectors. Strictly speaking, this only makes sense if the detectors have identical PSDs, which is approximately true for the two LIGO detectors but not true in general. This simplifies the non-centrality parameter

$$\lambda = \mathcal{F}\mathcal{F}(\theta) \rho_{\text{opt}}^{\text{net}}(\theta). \quad (15)$$

Future iterations of our prescription could easily relax this assumption.

Figure 1 illustrates our procedure, which proceeds as follows. For each injection, we first compute the fitting factor $\mathcal{F}\mathcal{F}(\theta)$ for a given template bank. We then evaluate the optimal network SNR, $\rho_{\text{opt}}^{\text{net}}(\theta)$, and model the observed network SNR, $\hat{\rho}_{\text{obs},\phi}^{\text{net}}$, by drawing from a χ -distribution with $2N_{\text{det}}$ degrees of freedom and a non-centrality parameter $\lambda = \mathcal{F}\mathcal{F}(\theta) \rho_{\text{opt}}^{\text{net}}(\theta)$. This methodology deviates from actual search pipelines, which perform the maximization in the right-hand side of Equation (12) directly on the *noisy data*. In contrast, we maximize the signal response over the template bank prior to incorporating noise. These operations do not commute—specific noise realizations can shift the maximum SNR to a template distinct from the true best-match template. Nevertheless, we demonstrate in §3 that this approximation remains robust and accurate for the majority of scenarios and applications considered in this work.

For each injection, our prescription estimates $\hat{\rho}_{\text{obs},\phi}^{\text{net}}$ by calculating $\mathcal{F}\mathcal{F}(\theta)$ using a single reference PSD and separately computing $\rho_{\text{opt}}^i(\theta)$ for each detector to obtain the non-centrality parameter in Eq. 15. The former entails calculating a vast number of inner products, which traditionally poses a computational bottleneck ($\gtrsim 10^{12}$ inner products for a standard injection set and template bank; R. Essick et al. 2025). We overcome this limitation by employing GPU-compatible waveforms, implemented in the `ripple` software package (T. D. P. Edwards et al. 2024) via the `jax` array backend.

For the analyses presented in §3, we find that the time T required to compute $\mathcal{F}\mathcal{F}(\theta)$ on a single NVIDIA TITAN V GPU scales as:

$$\frac{T}{1 \text{ hr}} \approx \left(\frac{N_{\text{inj}}}{1.5 \times 10^4} \right) \left(\frac{N_{\text{temp}}}{10^6} \right) \left(\frac{\Delta f}{2 \text{ Hz}} \right) \quad (16)$$

where N_{inj} is the number of injections, N_{temp} is the number of templates, and Δf is the frequency grid spacing used to generate both the injections and templates (see also Appendix B). Once $\hat{\rho}_{\text{obs},\phi}^{\text{net}}$ is calculated for each injection, the only free parameter remaining to define detectability is the threshold ρ_{thr} placed on $\hat{\rho}_{\text{obs},\phi}^{\text{net}}$. It is possible to calibrate ρ_{thr} by comparing to real search results if they are available. For instance, R. Essick (2023) found $\rho_{\text{thr}} = 10$ by comparing semianalytic estimates to search estimates in O3 (R. Abbott et al. 2023; LIGO Scientific Collaboration et al. 2023). We fix $\rho_{\text{thr}} = 10$ throughout the paper, but see Appendix A for additional explorations in calibrating ρ_{thr} .

3. APPLICATIONS

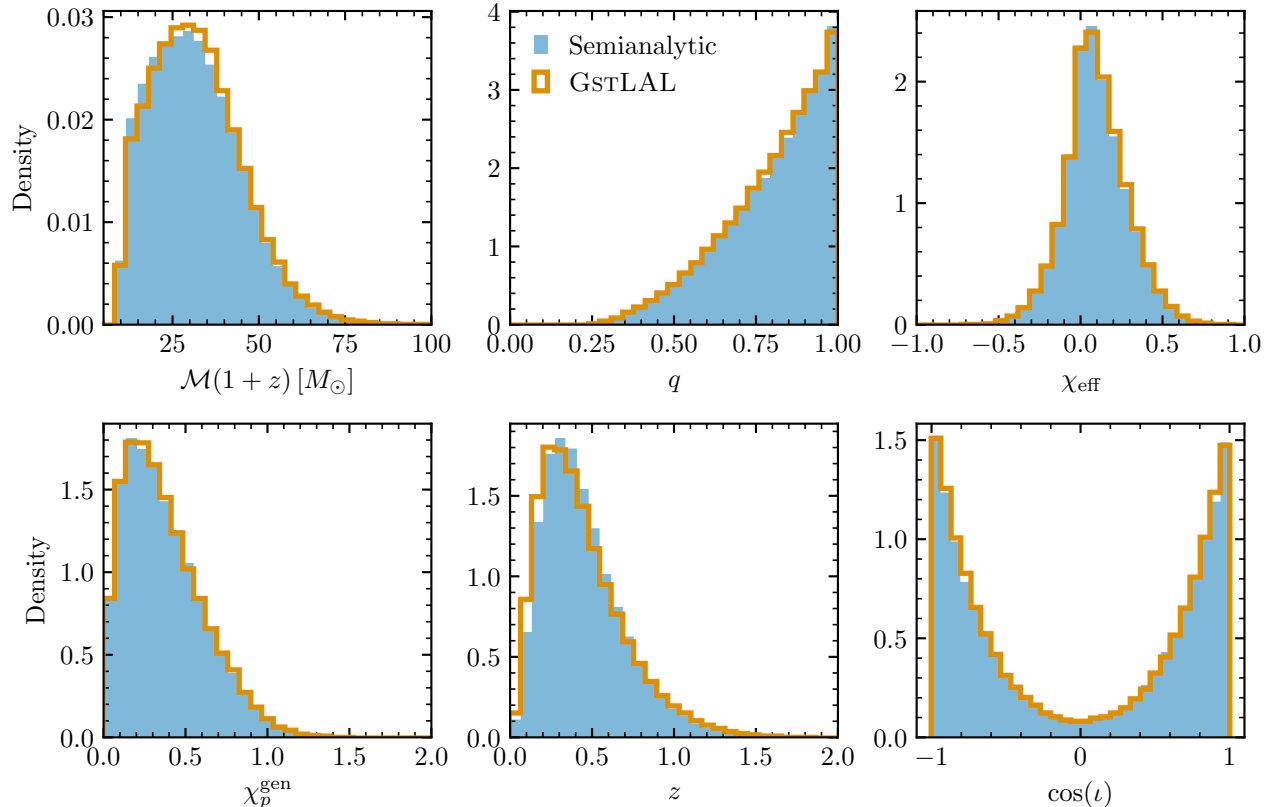


FIG. 2.— *Distributions of detected source parameters from the GSTLAL results and the semianalytic prescription.* We assume a population model following Equation (17) with $m_{\min} = 10 M_{\odot}$ and $m_{\max} = 40 M_{\odot}$. The distributions match between the semianalytic prescription and the real GSTLAL-inspiral search results.

In this section, we demonstrate the utility of our method by applying it to scenarios involving incomplete and finite template banks when all physics is known and included (§3.1), signals for which known physical effects are not included in the template bank (§3.2), and signals for which the full physical description is not necessarily known (§3.3). We use \mathcal{M} to denote chirp mass in the source frame, q to denote mass ratio, m_1 and m_2 to denote primary and secondary component masses in the source frame, M to denote total mass in the source frame, D_L to denote luminosity distance, z to denote redshift, χ_{eff} to denote the effective inspiral spin, ι to denote inclination of the orbit, χ_p^{gen} to denote generalized effective precessing spin (D. Gerosa et al. 2021), and e to denote eccentricity.

3.1. Discrete and Incomplete Template Banks

We first show that our semianalytic prescriptions can faithfully reproduce search behavior in the simplest case of discrete (but approximately complete) template banks. For this purpose, we construct a semianalytic injection set for BBHs, and compare it to GSTLAL sensitivity es-

timates from the first part of the LVK’s fourth observing run (O4a) (A. G. Abac et al. 2025). The injection set that the sensitivity estimates were run on as well as our semianalytic injection set assume IMRPHENOMXPHM (G. Pratten et al. 2021) as the waveform approximant, and this approximant includes the effects of precession as well as higher modes on the signal. However, the template bank of GSTLAL and other searches in O4 (K. Cannon et al. 2012; C. Messick et al. 2017; S. Roy et al. 2017a,b; C. Hanna et al. 2020; K. Cannon et al. 2021; S. Sakon et al. 2024; A. Ray et al. 2023; L. Tsukada et al. 2023; B. Ewing et al. 2024; P. Joshi et al. 2025a,b; C. All  n   et al. 2025; T. Dal Canton et al. 2021; Q. Chu et al. 2022) assume aligned-spin signals. While this does lead to some loss in sensitivity, it has been shown that the loss is small for most regions in the parameter space (I. Harry et al. 2016, 2018). In any case, our semianalytic prescription can pick up on these differences if they were to be large.

To compare our semianalytic injection set to the one produced for O4a, we reweigh all our results to a fiducial mass model given by $p(m_1, m_2 | m_{\min}, m_{\max}) = p(m_1 | m_{\min}, m_{\max})p(m_2 | m_1, m_{\min}, m_{\max})$ where

$$\begin{aligned}
 p(m_1 | m_{\min}, m_{\max}) &= \frac{m_1^{-1}}{\ln\left(\frac{m_{\max}}{m_{\min}}\right)} ; m_{\min} \leq m_1 \leq m_{\max} \\
 &= 0 ; \text{otherwise}
 \end{aligned}$$

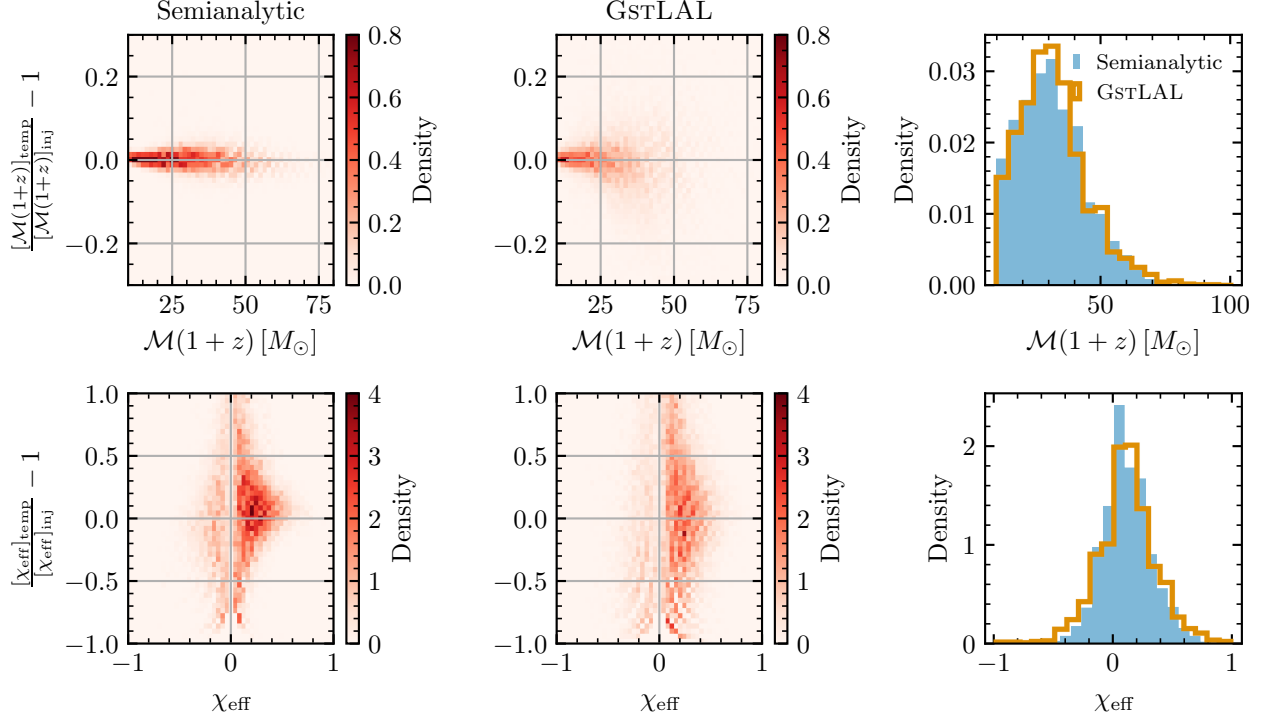


FIG. 3.— *Distribution of best-match template parameters for $m_{\min} = 10 M_{\odot}$ and $m_{\max} = 40 M_{\odot}$.* In the first row, the first panel shows the histogram of the injected $\mathcal{M}(1+z)$ (horizontal axis) and the fractional error (vertical axis) for the semianalytic estimates. The ‘inj’ and ‘temp’ subscripts refer to the injected value and the corresponding recovered template value respectively. The second panel shows the same quantities as the first panel but for the actual GSTLAL search results. The third panel compares the distribution of recovered templates in our semianalytic estimates and from GSTLAL search results. All the results have similar trends between the semianalytic and GSTLAL results, with differences increasing towards high mass.

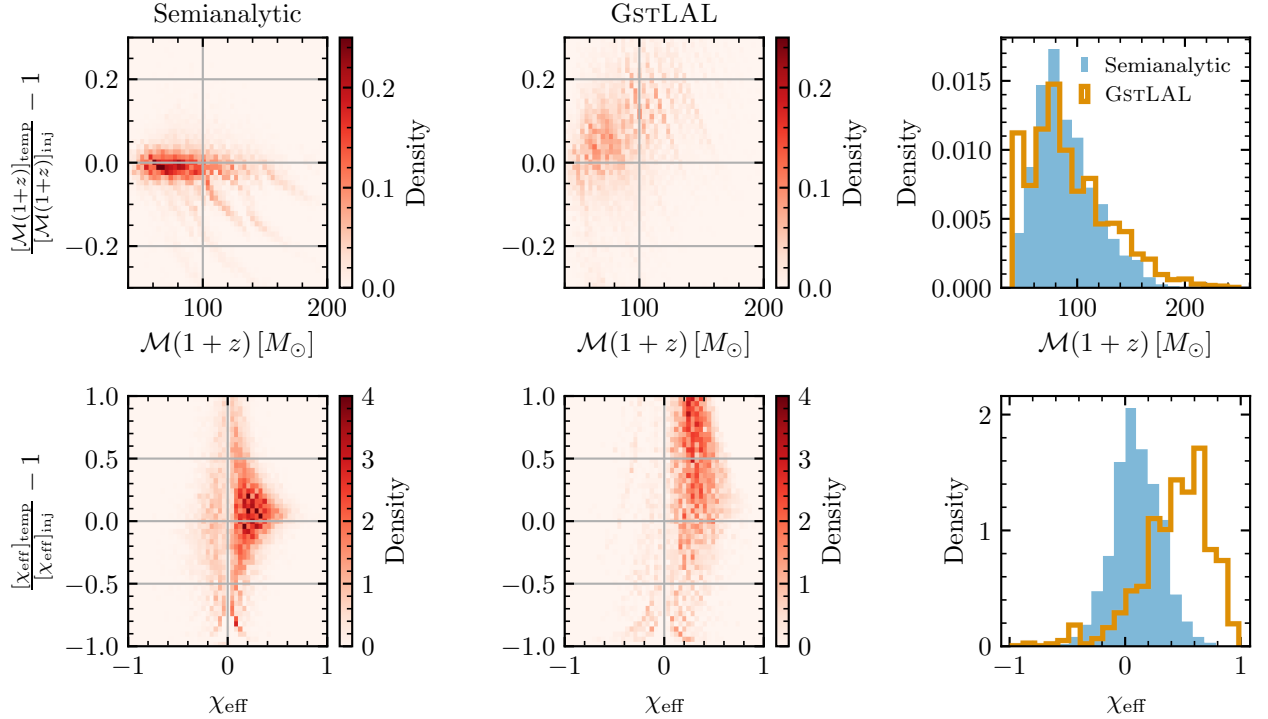


FIG. 4.— *Distribution of best-match template parameters for $m_{\min} = 40 M_{\odot}$ and $m_{\max} = 100 M_{\odot}$.* The panels describe the same quantities as those in Figure 3. However, we see significant differences in the template parameters, especially for χ_{eff} .

$$p(m_2|m_1, m_{\min}, m_{\max}) = \frac{2m_2}{m_1^2 - m_{\min}^2} \Theta(m_{\min} \leq m_2 \leq m_1). \quad (17)$$

The distribution of all other parameters is held fixed to the fiducial choices made in the injection set. In Figure 2, we compare the detected distributions under Equation 17 with parameters $m_{\min} = 10 M_{\odot}$ and $m_{\max} = 40 M_{\odot}$. We find that the detected distribution agree, similar to the results of R. Essick (2023).

A useful byproduct of the $\mathcal{FF}(\theta)$ calculation is an estimate of the best-match template parameters. In Figures 3 and 4, we compare the recovered templates from the actual GSTLAL search to our semianalytic approximation for two injected populations: one with $m_{\min} = 10 M_{\odot}$ and $m_{\max} = 40 M_{\odot}$, and another with $m_{\min} = 40 M_{\odot}$ and $m_{\max} = 100 M_{\odot}$. We find that the distributions of $\mathcal{M}(1+z)$, and the mass ratio, q , for the best-match templates show good agreement between our semianalytic prescription and the real GSTLAL injections. However, while the effective spin (χ_{eff}) distributions of the best-match templates align closely for the low-mass population, they diverge significantly for the high-mass population. While we did not investigate the reason for the discrepancy in detail, it is likely to be related to other operations in GSTLAL that we do not emulate e.g., data conditioning, signal consistency tests. For instance, non-Gaussian noise artifacts could preferentially respond to the shorter negative χ_{eff} templates, substantially enhancing the noise background at those templates and shifting the preferred event to positive χ_{eff} values. Nevertheless, these estimates of template parameters may be valuable; for instance, they can be utilized in population analyses that apply parameter cuts to probe specific features in the binary black hole mass distribution (S. Kishore Roy et al. 2025), or to mimic mass thresholds used for selecting events in certain tests of general relativity (The LIGO Scientific Collaboration et al. 2026c).

Search template banks are constructed to target specific fiducial source populations, a choice typically motivated by astrophysical priors. A notable example is the low-mass region of the GSTLAL template banks (D. Mukherjee et al. 2021; R. Abbott et al. 2021; S. Sakon et al. 2024), which does not include support for effective spins of $|\chi_{\text{eff}}| > 0.05$ at redshifted chirp masses $\mathcal{M}(1+z) \lesssim 1.5 M_{\odot}$. This boundary is adopted because binary neutron stars with such high spins that will merge within a Hubble time have not been observed in the Milky Way (M. Kramer & N. Wex 2009). Similar gaps exist in the template banks of other search pipelines (T. Dal Canton & I. W. Harry 2017; C. All  n   et al. 2025). Consequently, these searches should exhibit reduced sensitivity to signals occupying such gaps in the parameter space.

To illustrate this effect, we use the BNS injection set used for sensitivity estimates during the LVK’s third observing run (O3) (LIGO Scientific Collaboration et al. 2023; R. Abbott et al. 2023). The O3 injection set has a larger number of BNS injections compared to the O4a injection set, allowing for a stricter test of our prescription. We plot the fraction of detected signals with redshifted chirp masses $\mathcal{M}(1+z) < 1.5 M_{\odot}$, applying a false alarm rate threshold of $\text{FAR} < 1 \text{ yr}^{-1}$ to the real search results. As shown in Figure 5, the search data demonstrates a clear degradation in sensitivity as χ_{eff} deviates from zero. Our semianalytic prescription successfully reproduces this

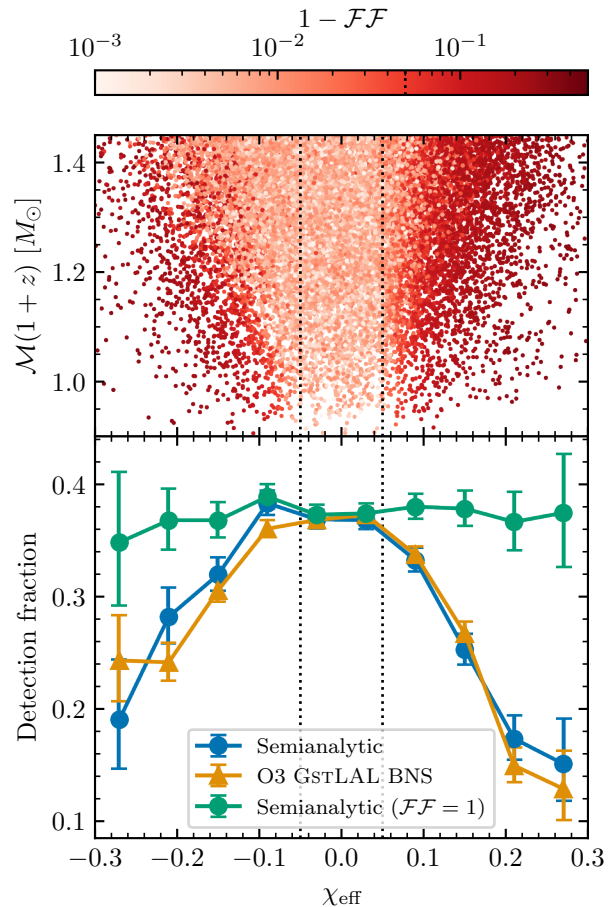


FIG. 5.— *Gaps in the template bank.* The top panel shows the $1 - \mathcal{FF}$ values for BNS injections in O3 with $\mathcal{M}(1+z) < 1.45$. While \mathcal{FF} is large for points with $|\chi_{\text{eff}}| < 0.05$, it drops sharply outside this range. This is a direct consequence of the lack of templates with $|\chi_{\text{eff}}| > 0.05$ points in the GSTLAL template bank. In the bottom panel, we show the detection fraction of these injections as a function of χ_{eff} also comparing it to results from the GSTLAL search in O3. The detection fraction drops steeply beyond $|\chi_{\text{eff}}| > 0.05$, dropping by a factor of > 3 at $\chi_{\text{eff}} = 0.3$. The semianalytic sensitivity curves (orange) tracks the real search results (blue) within their uncertainty regions. Semianalytic sensitivity estimates that assume $\mathcal{FF}(\theta) = 1$ (green) [Equations (13) and (14)] fail to capture this trend.

trend. For our model, we assume a three-detector network (HLV) utilizing the representative O3 PSD from LIGO Scientific Collaboration et al. (2025). We adopt the O3 GSTLAL template bank (R. Abbott et al. 2021) and use an injection distribution identical to that in R. Abbott et al. (2023). To compare our predictions directly with the real search results, we apply a threshold of $\rho_{\text{thr}} = 10$ on $\hat{\rho}_{\text{obs},\phi}^{\text{net}}$. Our derived detection fractions closely align with the empirical search results and shows that sensitivity degrades more severely for positive χ_{eff} than for negative χ_{eff} . This asymmetry is primarily driven by the orbital hangup effect (M. Campanelli et al. 2006): systems with positive χ_{eff} inspiral for a larger number of cycles, and vice versa for negative χ_{eff} systems. Because the template bank lacks templates at high positive spins,

the search algorithm attempts to recover these signals using templates with lower chirp masses to compensate for the extra cycles. However, this compensation is imperfect due to differing dependence of the dominant terms involving \mathcal{M} and χ_{eff} in the post-Newtonian expansion, and the ability to shift to a lower chirp mass is strictly bounded by the low-mass edge of the template bank. In contrast, the bank extends to much higher chirp masses, providing ample templates to absorb the shorter waveforms of negative χ_{eff} systems. This explains the comparatively smaller drop in sensitivity for negative spins. The sensitivity drops by a factor of ~ 2 at $\chi_{\text{eff}} \approx 0.2$, worsening to a factor of > 3 for systems reaching $\chi_{\text{eff}} \approx 0.3$.

During the LVK’s fourth observing run (O4), no unretracted public alerts (LIGO Scientific Collaboration et al. 2026) were issued for BNSs. Consequently, the estimated BNS merger rates have been revised downward in the latest catalog when compared to the estimates following the detection of GW170817 (The LIGO Scientific Collaboration et al. 2025b). While there are a number of well-motivated astrophysical explanations for this dearth of detections (M. Fishbach et al. 2026; K. Kunnunkai et al. 2026), one speculative proposal in the context of the result in Figure 5 is that there exists a significant population of BNSs at high spin that the template bank considered here is not adequately equipped to detect¹.

3.2. Known Missing Physics

Detecting imprints of orbital eccentricity in GW signals is one of the big goals for GW astronomy. Apart from having rich features from a phenomenological standpoint, eccentric mergers are also excellent tracers of the progenitor environments of compact binaries. GW emission is very efficient at radiating away eccentricity from a binary system (P. C. Peters 1964). Thus, to retain any semblance of eccentricity in the band of the LVK detectors, the binary should have formed at low separations but with high eccentricities. Dense star clusters (e.g., F. Antonini & F. A. Rasio 2016; C. L. Rodriguez et al. 2018; G. Fragione et al. 2019; L. Gondán et al. 2018; F. Antonini & M. Gieles 2020; M. Dall’Amico et al. 2024), hierarchical triple systems (e.g., L. Wen 2003; K. Silsbee & S. Tremaine 2017; F. Antonini et al. 2017; A. Dorozzmai et al. 2026), disks of active galactic nuclei (e.g., Y. Yang et al. 2019; J. Samsing et al. 2022), etc., provide natural settings to host such mergers. Spurred by their astrophysical significance, there have been a number of efforts in recent years to model the waveforms of eccentric signals (A. Gamboa et al. 2025; G. Morras et al. 2025; S. Albanesi et al. 2025; M. d. L. Planas et al. 2026; A. Ramos-Buades et al. 2026).

We illustrate the selection function for nonspinning, eccentric BNSs by creating injection set using the TAYLORF2ECC waveform approximant (B. Moore et al. 2016) over a narrow range of eccentricities 0-0.2. BNS signals are long and hence are amenable to measurements of smaller values of orbital eccentricity as compared to BBHs (M. Zevin et al. 2021; A. Vijaykumar et al. 2024). This same fact also means that the detectability of eccentric signals drops sharply for nonzero eccentricities, when

¹ Other flavors of searches such as the GSTLAL search for sub-solar mass objects (C. Hanna et al. 2025) could be sensitive to high spin configurations.

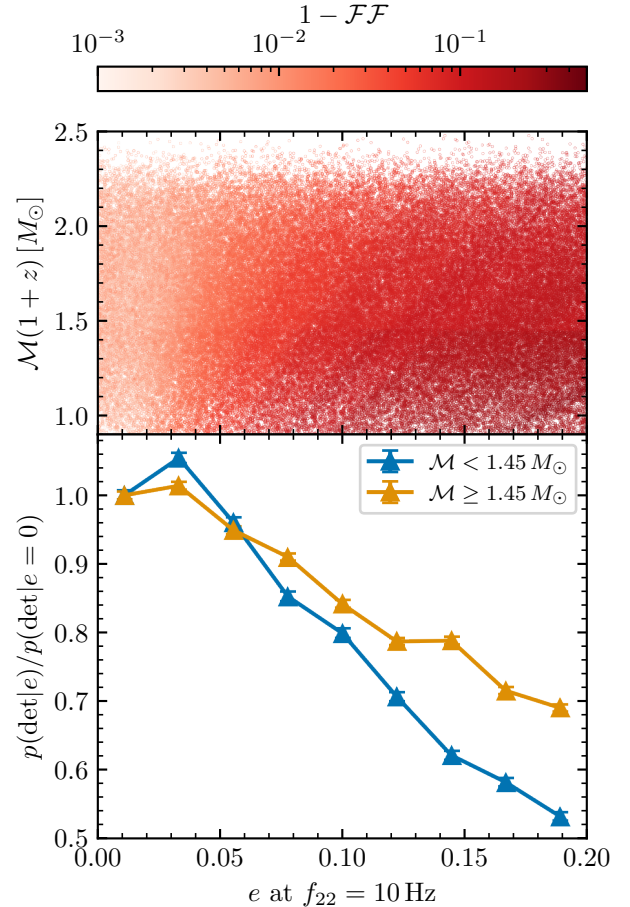


FIG. 6.— Semianalytic sensitivity estimates for nonspinning, eccentric BNS systems. The top panel shows values of $1 - \mathcal{FF}$ in the $\mathcal{M}(1+z)$ - e space, where the eccentricity e is defined at dominant (2,2) mode frequency of 10 Hz. The \mathcal{FF} values decrease with increasing e . In the bottom panel, we plot the ratio $p(\text{det}|e)/p(\text{det}|e=0)$ in different eccentricity bins for two different BNS mass bins.

recovered with a template bank that contains circular signals. This is also evident from Figure 6, where we see around a factor of $\sim 20\%$ drop in sensitivity at $e \approx 0.1$ and $\sim 30\text{-}50\%$ drop in sensitivity at $e \approx 0.2$ depending on the chirp mass range. Thus, if BNS signals have a small residual eccentricity due to being part of a hierarchical triple system (A. S. Hamers & T. A. Thompson 2019) or being produced by through specific natal kick configurations (P. Beniamini & T. Piran 2024), a significant fraction will be missed by the current LVK search pipelines. Thus, searches with orbital eccentricity (A. H. Nitz & Y.-F. Wang 2021; R. Dhurkunde & A. H. Nitz 2025; K. Kacanja et al. 2025; K. S. Phukon et al. 2026) are timely.

To test for sensitivity to eccentric BBHs, we use results from B. Gadre et al. (2024) as a point of comparison. B. Gadre et al. (2024) examine the sensitivity of the PYCBC search pipeline in O3 to eccentric signals. For this purpose, they create an injection set with a range of masses between $\mathcal{M}(1+z) \in [5, 70] M_{\odot}$ and eccentricities between 0-0.6 using the SEOBNRv5EHM waveform approximant (A. Gamboa et al. 2025). Luminosity distances are distributed uniformly in chirp distance i.e.,

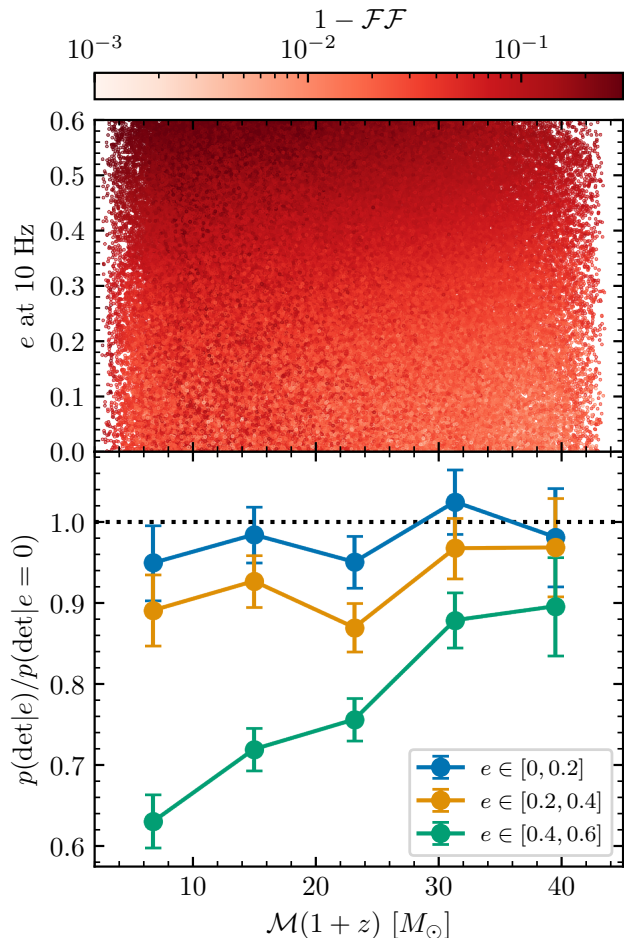


FIG. 7.— *Semianalytic sensitivity estimates for aligned-spin, eccentric BBH systems.* The top panel shows the recovered $1 - \mathcal{FF}$ values in the e - $\mathcal{M}(1+z)$ plane for an injection set statistically identical to the one used in B. Gadre et al. (2024). The bottom panel shows the ratio $p(\text{det}|e)/p(\text{det}|e=0)$ for different eccentricity ranges and in different bins of $\mathcal{M}(1+z)$.

$D_L[\mathcal{M}(1+z)/M_\odot]^{5/6}$, between 5 Mpc and 300 Mpc. The eccentricity is defined at a reference 22-mode GW frequency of 10 Hz. We create a statistically identical injection set (albeit with a larger number of injections), and calculate $\hat{\rho}_{\text{obs},\phi}^{\text{net}}$ assuming the PYCBC template bank and PSDs that were used for the search. In Figure 7, we plot the ratio $p(\text{det}|e)/p(\text{det}|e=0)$ as a function of the injection chirp mass, where the ratio quantifies the probability in a certain bin of eccentricity divided by the detection probability for circular signals under the same distributions for the other source parameters. We are able to reproduce the 5%-30% drops in sensitivity observed across eccentricities for a range of masses.

3.3. Unknown Missing Physics

Yet another example of missing physics in template banks is that of effects beyond general relativity. Understanding the selection effects inherent for signals from theories beyond general relativity is important when combining information from multiple events in hierarchical tests of general relativity (M. Isi et al. 2019).

For the purposes of this subsection, we follow R. Magee et al. (2024) and use the results therein as a point of

comparison. The inspiral dynamics of a compact binary merger can be approximated by post Newtonian (PN) theory. Following post-Newtonian theory, the GW phase can be expanded as a series in orbital velocity v . That is, the GW phase in general relativity can be written as,

$$\psi(v) = -\frac{3}{128\eta}v^{-5} \sum_k \phi_k v^k \quad (18)$$

where ϕ_k is the PN coefficient corresponding to order k . In general relativity, k can take values 0, 2, 3, 4, ... One can add *fractional* deviations by parameterizing $\phi_k \rightarrow \phi_k(1 + \delta\phi_k)$ for these orders, and absolute deviations $\delta\phi_k$ for orders that do not appear in general relativity. Here, we will only consider the deviations at orders $k = -2$ and $k = 1$.

We use exactly the same population as in R. Magee et al. (2024) and plot the histogram of detected injections, assuming the O3 GSTLAL template banks and PSDs. The histogram in R. Magee et al. (2024) showed fewer detected signals at negative values of $\delta\phi_{-2}$ compared to positive values. This asymmetry arises because negative $\delta\phi_{-2}$ values correspond to longer signals, leading to more waveform cycles; as a result, the template banks is efficient at recovering such signals. This trend is also borne out in our semianalytic sensitivity estimates plotted in Figure 8. There are also strong trends as a function of total mass with greater loss in detections at extreme values of $\delta\phi_{-2}$. Similar trends are visible for $\delta\phi_1$. This loss in sensitivity may be ameliorated by designing searches to detect beyond-GR deviations (e.g., H. Narola et al. 2023; A. Sharma et al. 2024).

4. DISCUSSION

There are a number of other approaches in the literature aimed at fast evaluation of selection effects. One class of such methods abandons physical understanding of the selection function and attempts to fit a (over)parametrized model directly from injections using machine learning techniques (D. Gerosa et al. 2020; C. Talbot & E. Thrane 2020; T. A. Callister et al. 2024). While these approaches can capture selection biases arising from unmodeled effects in the template bank, they require that injections be processed through a full search pipeline, and thus inherit the same computational and person-power challenges as real search analyses. They also will not necessarily generalize well, manifestly cannot capture effects that were not in the original injection set, and have many free parameters that often have no clear interpretation. Other methods that calibrate injections processed by searches to expressions that are simple to evaluate (M. Mould et al. 2024; A. Lorenzo-Medina & T. Dent 2025) suffer from the same issues.

Another set of methods (L. S. Finn & D. F. Chernoff 1993; D. Wysocki et al. 2019; D. Gerosa & M. Bellotti 2024) use physical principles behind the signal model and detection process, similar in principle to R. Essick (2023). These are expected to generalize better and some have relatively few free parameters (e.g., R. Essick 2023 has only a single free parameters: ρ_{thr}). While these approaches may be able to capture effects not originally included in injection sets processed by searches, they assume that the template bank is dense and complete. Therefore, they cannot account for any of the effects considered in

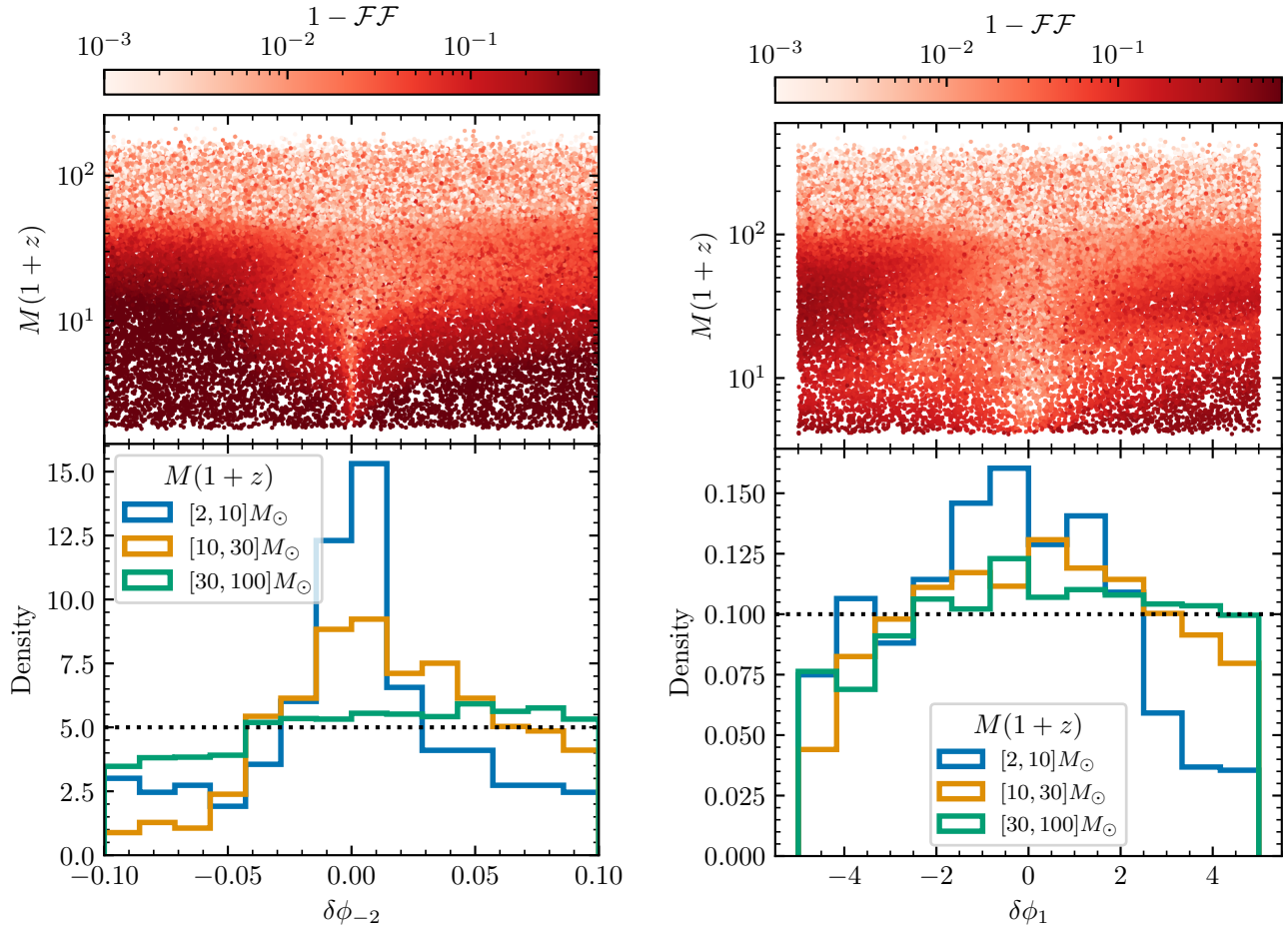


FIG. 8.— *Semianalytic sensitivity estimates for BBH systems with deviations away from general relativity.* The top panels show the values of $1 - \mathcal{FF}$ in the $M(1+z)$ - $\delta\phi$ parameter space. The bottom panels show the detected distributions for the $\delta\phi_{-2}$ and $\delta\phi_1$ deviation parameters in three different mass bins.

§3. The methods developed in this work alleviate both these issues and enable fast evaluation of the selection function for a large class of signals. The injection set thus generated could also be used to train neural network emulators (T. A. Callister et al. 2024), particularly for use in simulation-based inference frameworks (K. Leyde et al. 2026).

We emphasize that the semianalytic sensitivity estimates presented here do not replicate the full behaviour of a search pipeline; rather, they approximate only the matched-filtering operation. Real searches apply a suite of signal consistency tests to construct their detection statistics, like PyCBC’s newsnr (S. Babak et al. 2013) and GstLAL’s autocorrelation ξ^2 (L. Tsukada et al. 2023) to verify the consistency of signal power across frequency bins. These tests are designed to suppress instrumental artefacts and are not expected to affect genuine compact binary signals. Consistent with this expectation, our results indicate that signal-consistency tests have only a minor impact on injection-based sensitivity estimates and that sensitivity is primarily driven by SNR loss from template mismatch. Nonetheless, signals that are highly eccentric or that deviate substantially from the GR waveform manifold may fail χ^2 -like consistency tests. Consequently, our semianalytic estimates should be interpreted as upper limits on the achievable search sen-

sitivity. Similar conclusions were reported by R. Magee et al. (2024) in their analysis of signals beyond general relativity using real search pipelines.

Throughout this work, we have assumed that the $\mathcal{FF}(\theta)$ value and the corresponding best match template are the same across detectors. This may not be strictly true, since detectors that have different PSD shapes would give different values of $\mathcal{FF}(\theta)$. Additionally, we have assumed fixed representative PSDs for ease of computation, but this condition can also be relaxed. The results of §3 suggest that these assumptions are unlikely to introduce a significant bias, although a more general version of the prescription used in this paper can be incorporated in future extensions.

Our framework identifies the best-match template by maximizing the match over template parameters before projecting onto a detector network and introducing the effects of noise. This contrasts with actual search pipelines, which operate on the SNR of the noisy data across the template bank. However, this simplification is well-justified; as demonstrated by R. Essick (2023), the strong correlations present across the template bank ensure that this approximation yields reliable estimates for $\hat{\rho}_{\text{obs},\phi}^{\text{net}}$ and the overall detectability. Additionally, we find that the inherent discreteness of template banks means this noise-

free maximization approach also serves as a reasonable approximation for recovering the best-match template parameter.

This work only considers quadrupolar aligned-spin template banks, consistent with the template banks employed in the searches we reference. This assumption also simplifies the computation of $\mathcal{FF}(\theta)$. There is, however, no fundamental obstacle to extending our framework to searches such as the IAS-HM search (D. Wadekar et al. 2024). In that case, the data are independently filtered with templates corresponding to different harmonics, and the resulting detection statistics are subsequently combined in post-processing. A similar strategy could be implemented within our semianalytic prescription, although doing so would increase the computational cost by approximately a factor equal to the number of harmonics considered. Similar prescriptions can be applied to searches that model eccentricity and precession in their template banks.

Our prescription can be used to rapidly identify sensitivity gaps across the parameter to specific class of signals, and can be extended to a variety of applications including gravitational lensing (J. C. L. Chan et al. 2025), astrophysics-induced modulation of the signal (e.g., A. Vijaykumar et al. 2023; S. Roy & R. Vicente 2025; A. Tiwari et al. 2025), and a wide variety of effects beyond Kerr and general relativity.

ACKNOWLEDGEMENTS

APPENDIX

MASS-DEPENDENT SNR THRESHOLD

We investigate if there is evidence for a mass-dependent SNR threshold ρ_{thr} when calibrating the semianalytic estimates against real GSTLAL results from O4a. In order to find the optimal threshold in each mass bin, we compare the redshift distributions of our semianalytic estimates under different SNR threshold to injections detected with $\text{FAR} < 1 \text{ yr}^{-1}$ in GSTLAL.

Let $g(z)$ denote the redshift distribution from GSTLAL and $s(z|\bar{\rho})$ denote the redshift distribution from the semianalytic estimate under a certain SNR threshold $\bar{\rho}$. Let $G(z)$ and $S(z|\bar{\rho})$ be the corresponding cumulative density functions respectively. To quantify the match between distributions, we calculate two different quantities:

1. **Wasserstein distance:** $W(g, s; \bar{\rho}) = \int dz |G(z) - S(z|\bar{\rho})|$. Also sometimes referred to as the “earth mover’s distance”.
2. **Kullback-Leibler (KL) Divergence:** $D_{\text{KL}}(g, s; \bar{\rho}) = \int dz g(z) \log \frac{g(z)}{s(z|\bar{\rho})}$

The optimal threshold ρ_{thr} is the value of $\bar{\rho}$ that minimizes $W(g, s; \bar{\rho})$ or $D_{\text{KL}}(g, s; \bar{\rho})$. We plot the derived results in Figure 9. Regardless of whether we minimize the Wasserstein distance or the KL divergence, ρ_{thr} is constant above $\approx 30 M_{\odot}$ but rises below that value. The ρ_{thr} values derived using the KL divergence are systematically lower than the ones derived using the Wasserstein distance. This may be attributed to how these metrics pick up on differences between distributions. The Wasserstein distance is minimized when the bulk of the distribution is similar, since a low probability tail of the distribution doesn’t impact the CDF significantly. However, the KL divergence is highly sensitive to such a tail—if $g(z)$ has finite but small support at large redshifts but $s(z|\bar{\rho})$ has zero support, D_{KL} is driven to very high values. A smaller $\bar{\rho}$ places more mergers at high redshift, thus reducing the value of the KL divergence and driving ρ_{thr} to smaller values.

INSENSITIVITY OF THE FITTING FACTOR TO SPACING OF THE FREQUENCY GRID

While calculating the fitting factor, one maximizes the overlap across the relative time offset t_0^* between the candidate signal and the data. This time-maximization is performed by taking the inverse Fast Fourier Transform (IFFT) of the noise-weighted inner product of the candidate signal and the data. Assuming the minimum and maximum frequencies on the frequency grid are f_{min} and f_{max} , respectively, and the grid spacing is Δf , the resolution of the IFFT time grid

We thank Shio Sakon for many useful discussions about GSTLAL template banks and analysis choices, and for a careful reading of our draft. We also thank Kanchan Soni and Bhooshan Gadre for clarifications about B. Gadre et al. (2024) and sharing the template bank used in that work. We are grateful to Bart Ripperda for graciously granting us access to the GPU-enabled BEE workstation at CITA. This research has made use of the Astrophysics Data System, funded by NASA under Cooperative Agreement 80NSSC21M00561.

This research was supported by the Natural Sciences and Engineering Research Council of Canada (NSERC). R.E. is supported by NSERC Grant RGPIN-2023-03346, and A.V. is supported by NSERC Grant DIS-2022-568580. We acknowledge the use of the following software packages: `gw-detectors` (R. Essick 2025), `gw-distributions` (R. Essick et al. 2025), `astropy` (Astropy Collaboration et al. 2013, 2018, 2022), `Jupyter` (F. Perez & B. E. Granger 2007; T. Kluyver et al. 2016), `matplotlib` (J. D. Hunter 2007), `numpy` (C. R. Harris et al. 2020), `pandas` (Wes McKinney 2010; T. pandas development team 2025), `python` (G. Van Rossum & F. L. Drake 2009), `scipy` (P. Virtanen et al. 2020; R. Gommers et al. 2025), `Cython` (S. Behnel et al. 2011), `h5py` (A. Collette 2013; A. Collette et al. 2023), `JAX` (J. Bradbury et al. 2018), `LALSuite` (LIGO Scientific Collaboration et al. 2018; K. Wette 2020), `seaborn` (M. L. Waskom 2021), `OverCite` (C. Shariat 2026), and `tqdm` (C. da Costa-Luis et al. 2024). Part of the software citation information was aggregated using `The Software Citation Station` (T. Wagg & F. S. Broekgaarden 2024; T. Wagg et al. 2025).

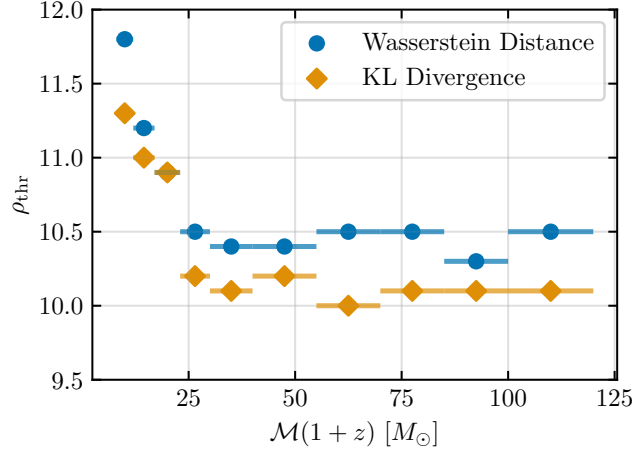


FIG. 9.— SNR threshold ρ_{thr} calibrated to GSTLAL results as a function of detector frame chirp mass.

is $(f_{\text{max}} - f_{\text{min}})^{-1} \approx 1$ ms, and its length is $1/(\Delta f)$. For a typical template bank, t_0^* is $\mathcal{O}(10\text{--}100)$ ms, which can be very well resolved with the ≈ 1 ms resolution. Further, because the resolution of the time grid is independent of the frequency grid spacing, one can choose a large Δf and still obtain an accurate match and fitting factor. This drastically reduces computational cost, which scales inversely with Δf . Increasing Δf naturally introduces a numerical discretization error in the match calculation; however, this error is expected to be quite small, even when using $\Delta f = 4$ Hz.

To test this empirically, we calculated the fitting factors for nonspinning, equal-mass binary black hole mergers with chirp masses between $6 M_{\odot}$ and $100 M_{\odot}$ using $\Delta f = 1/16$ Hz and $\Delta f = 4$ Hz. The maximum absolute difference in the resulting fitting factors was found to be 0.005, which is negligible for all purposes of this work.

REFERENCES

- Abac, A. G., Abouelfettouh, I., Acernese, F., et al. 2025, GWTC-4.0: An Introduction to Version 4.0 of the Gravitational-Wave Transient Catalog, *ApJ*, 995, L18, doi: [10.3847/2041-8213/ae0c06](https://doi.org/10.3847/2041-8213/ae0c06)
- Abbott, R., Abbott, T. D., Abraham, S., et al. 2021, GWTC-2: Compact Binary Coalescences Observed by LIGO and Virgo during the First Half of the Third Observing Run, *Physical Review X*, 11, 021053, doi: [10.1103/PhysRevX.11.021053](https://doi.org/10.1103/PhysRevX.11.021053)
- Abbott, R., Abbott, T. D., Acernese, F., et al. 2023, Population of Merging Compact Binaries Inferred Using Gravitational Waves through GWTC-3, *Physical Review X*, 13, 011048, doi: [10.1103/PhysRevX.13.011048](https://doi.org/10.1103/PhysRevX.13.011048)
- Acernese, F., Agathos, M., Agatsuma, K., et al. 2015, Advanced Virgo: a second-generation interferometric gravitational wave detector, *Classical and Quantum Gravity*, 32, 024001, doi: [10.1088/0264-9381/32/2/024001](https://doi.org/10.1088/0264-9381/32/2/024001)
- Akutsu, T., Ando, M., Arai, K., et al. 2021, Overview of KAGRA: Detector design and construction history, *Progress of Theoretical and Experimental Physics*, 2021, 05A101, doi: [10.1093/ptep/ptaa125](https://doi.org/10.1093/ptep/ptaa125)
- Albanesi, S., Gamba, R., Bernuzzi, S., et al. 2025, Effective-one-body modeling for generic compact binaries with arbitrary orbits, *Phys. Rev. D*, 112, L121503, doi: [10.1103/3snf-w1x7](https://doi.org/10.1103/3snf-w1x7)
- All  n  , C., Aubin, F., Bentara, I., et al. 2025, The MBTA pipeline for detecting compact binary coalescences in the fourth LIGO-Virgo-KAGRA observing run, *Classical and Quantum Gravity*, 42, 105009, doi: [10.1088/1361-6382/add234](https://doi.org/10.1088/1361-6382/add234)
- Antonini, F., & Gieles, M. 2020, Population synthesis of black hole binary mergers from star clusters, *MNRAS*, 492, 2936, doi: [10.1093/mnras/stz3584](https://doi.org/10.1093/mnras/stz3584)
- Antonini, F., & Rasio, F. A. 2016, Merging Black Hole Binaries in Galactic Nuclei: Implications for Advanced-LIGO Detections, *ApJ*, 831, 187, doi: [10.3847/0004-637X/831/2/187](https://doi.org/10.3847/0004-637X/831/2/187)
- Antonini, F., Toonen, S., & Hamers, A. S. 2017, Binary Black Hole Mergers from Field Triples: Properties, Rates, and the Impact of Stellar Evolution, *ApJ*, 841, 77, doi: [10.3847/1538-4357/aa6f5e](https://doi.org/10.3847/1538-4357/aa6f5e)
- Apostolatos, T. A. 1995, Search templates for gravitational waves from precessing, inspiraling binaries, *Phys. Rev. D*, 52, 605, doi: [10.1103/PhysRevD.52.605](https://doi.org/10.1103/PhysRevD.52.605)
- Astropy Collaboration, Robitaille, T. P., Tollerud, E. J., et al. 2013, Astropy: A community Python package for astronomy, *A&A*, 558, A33, doi: [10.1051/0004-6361/201322068](https://doi.org/10.1051/0004-6361/201322068)
- Astropy Collaboration, Price-Whelan, A. M., Sip  cz, B. M., et al. 2018, The Astropy Project: Building an Open-science Project and Status of the v2.0 Core Package, *AJ*, 156, 123, doi: [10.3847/1538-3881/aabc4f](https://doi.org/10.3847/1538-3881/aabc4f)
- Astropy Collaboration, Price-Whelan, A. M., Lim, P. L., et al. 2022, The Astropy Project: Sustaining and Growing a Community-oriented Open-source Project and the Latest Major Release (v5.0) of the Core Package, *ApJ*, 935, 167, doi: [10.3847/1538-4357/ac7c74](https://doi.org/10.3847/1538-4357/ac7c74)
- Babak, S., Biswas, R., Brady, P. R., et al. 2013, Searching for gravitational waves from binary coalescence, *Phys. Rev. D*, 87, 024033, doi: [10.1103/PhysRevD.87.024033](https://doi.org/10.1103/PhysRevD.87.024033)
- Behnel, S., Bradshaw, R., Citro, C., et al. 2011, Cython: The Best of Both Worlds, *Computing in Science Engineering*, 13, 31, doi: [10.1109/MCSE.2010.118](https://doi.org/10.1109/MCSE.2010.118)
- Beniamini, P., & Piran, T. 2024, Ultrafast Compact Binary Mergers, *ApJ*, 966, 17, doi: [10.3847/1538-4357/ad32cd](https://doi.org/10.3847/1538-4357/ad32cd)
- Bradbury, J., Frostig, R., Hawkins, P., et al. 2018, JAX: composable transformations of Python+NumPy programs, 0.3.13 <http://github.com/google/jax>
- Callister, T. A., Essick, R., & Holz, D. E. 2024, Neural network emulator of the Advanced LIGO and Advanced Virgo selection function, *Phys. Rev. D*, 110, 123041, doi: [10.1103/PhysRevD.110.123041](https://doi.org/10.1103/PhysRevD.110.123041)
- Campanelli, M., Lousto, C. O., & Zlochower, Y. 2006, Spinning-black-hole binaries: The orbital hang-up, *Phys. Rev. D*, 74, 041501, doi: [10.1103/PhysRevD.74.041501](https://doi.org/10.1103/PhysRevD.74.041501)
- Cannon, K., Hanna, C., & Keppel, D. 2012, Interpolating compact binary waveforms using the singular value decomposition, *Phys. Rev. D*, 85, 081504, doi: [10.1103/PhysRevD.85.081504](https://doi.org/10.1103/PhysRevD.85.081504)
- Cannon, K., Caudill, S., Chan, C., et al. 2021, GstLAL: A software framework for gravitational wave discovery, *SoftwareX*, 14, 100680, doi: [10.1016/j.softx.2021.100680](https://doi.org/10.1016/j.softx.2021.100680)
- Chan, J. C. L., Seo, E., Li, A. K. Y., Fong, H., & Ezquiaga, J. M. 2025, Detectability of lensed gravitational waves in matched-filtering searches, *Phys. Rev. D*, 111, 084019, doi: [10.1103/PhysRevD.111.084019](https://doi.org/10.1103/PhysRevD.111.084019)
- Chu, Q., Kovalam, M., Wen, L., et al. 2022, SPIIR online coherent pipeline to search for gravitational waves from compact binary coalescences, *Phys. Rev. D*, 105, 024023, doi: [10.1103/PhysRevD.105.024023](https://doi.org/10.1103/PhysRevD.105.024023)
- Collette, A. 2013, Python and HDF5 (O'Reilly)
- Collette, A., Kluyver, T., Caswell, T. A., et al. 2023, h5py/h5py: 3.8.0, 3.8.0 Zenodo, doi: [10.5281/zenodo.7560547](https://doi.org/10.5281/zenodo.7560547)

- da Costa-Luis, C., Larroque, S. K., Altendorf, K., et al. 2024, tqdm: A fast, Extensible Progress Bar for Python and CLI, v4.67.1 Zenodo, doi: [10.5281/zenodo.14231923](https://doi.org/10.5281/zenodo.14231923)
- Dal Canton, T., & Harry, I. W. 2017, Designing a template bank to observe compact binary coalescences in Advanced LIGO's second observing run, arXiv e-prints, arXiv:1705.01845, doi: [10.48550/arXiv.1705.01845](https://doi.org/10.48550/arXiv.1705.01845)
- Dal Canton, T., Nitz, A. H., Gadre, B., et al. 2021, Real-time Search for Compact Binary Mergers in Advanced LIGO and Virgo's Third Observing Run Using PyCBC Live, ApJ, 923, 254, doi: [10.3847/1538-4357/ac2f9a](https://doi.org/10.3847/1538-4357/ac2f9a)
- Dall'Amico, M., Mapelli, M., Tormiamenti, S., & Arca Sedda, M. 2024, Eccentric black hole mergers via three-body interactions in young, globular, and nuclear star clusters, A&A, 683, A186, doi: [10.1051/0004-6361/202348745](https://doi.org/10.1051/0004-6361/202348745)
- Dhurkunde, R., & Nitz, A. H. 2025, Search for eccentric NSBH and BNS mergers in the third observing run of Advanced LIGO and Virgo, Phys. Rev. D, 111, 103018, doi: [10.1103/PhysRevD.111.103018](https://doi.org/10.1103/PhysRevD.111.103018)
- Dorozsmai, A., Romero-Shaw, I. M., Vijaykumar, A., et al. 2026, Hierarchical triples versus globular clusters: binary black hole merger eccentricity distributions compete and evolve with redshift, MNRAS, 545, staf1938, doi: [10.1093/mnras/staf1938](https://doi.org/10.1093/mnras/staf1938)
- Edwards, T. D. P., Wong, K. W. K., Lam, K. K. H., et al. 2024, Differentiable and hardware-accelerated waveforms for gravitational wave data analysis, Phys. Rev. D, 110, 064028, doi: [10.1103/PhysRevD.110.064028](https://doi.org/10.1103/PhysRevD.110.064028)
- Essick, R. 2023, Semianalytic sensitivity estimates for catalogs of gravitational-wave transients, Phys. Rev. D, 108, 043011, doi: [10.1103/PhysRevD.108.043011](https://doi.org/10.1103/PhysRevD.108.043011)
- Essick, R. 2025, gw-detectors, <https://git.ligo.org/reed.essick/gw-detectors>
- Essick, R., & Farr, W. 2022, Precision Requirements for Monte Carlo Sums within Hierarchical Bayesian Inference, arXiv e-prints, arXiv:2204.00461, doi: [10.48550/arXiv.2204.00461](https://doi.org/10.48550/arXiv.2204.00461)
- Essick, R., Coughlin, M. W., Zevin, M., et al. 2025, Compact binary coalescence sensitivity estimates with injection campaigns during the LIGO-Virgo-KAGRA Collaborations' fourth observing run, Phys. Rev. D, 112, 102001, doi: [10.1103/44x3-hv3y](https://doi.org/10.1103/44x3-hv3y)
- Essick, R., et al. 2025, gw-distributions, <https://git.ligo.org/reed.essick/gw-distributions>
- Ewing, B., Huxford, R., Singh, D., et al. 2024, Performance of the low-latency GstLAL inspiral search towards LIGO, Virgo, and KAGRA's fourth observing run, Phys. Rev. D, 109, 042008, doi: [10.1103/PhysRevD.109.042008](https://doi.org/10.1103/PhysRevD.109.042008)
- Finn, L. S., & Chernoff, D. F. 1993, Observing binary inspiral in gravitational radiation: One interferometer, Phys. Rev. D, 47, 2198, doi: [10.1103/PhysRevD.47.2198](https://doi.org/10.1103/PhysRevD.47.2198)
- Fishbach, M., Ji, A. P., Fong, W.-f., et al. 2026, Implications of low neutron star merger rates for gamma-ray bursts, r-process production and Galactic double neutron stars, arXiv e-prints, arXiv:2604.05059, doi: [10.48550/arXiv.2604.05059](https://doi.org/10.48550/arXiv.2604.05059)
- Fragione, G., Grishin, E., Leigh, N. W. C., Perets, H. B., & Perna, R. 2019, Black hole and neutron star mergers in galactic nuclei, MNRAS, 488, 47, doi: [10.1093/mnras/stz1651](https://doi.org/10.1093/mnras/stz1651)
- Gadre, B., Soni, K., Tiwari, S., et al. 2024, Detectability of eccentric binary black holes with matched filtering and unmodeled pipelines during the third observing run of LIGO-Virgo-KAGRA, Phys. Rev. D, 110, 044013, doi: [10.1103/PhysRevD.110.044013](https://doi.org/10.1103/PhysRevD.110.044013)
- Gamboa, A., Buonanno, A., Enficiaud, R., et al. 2025, Accurate waveforms for eccentric, aligned-spin binary black holes: The multipolar effective-one-body model SEOBNRv5EHM, Phys. Rev. D, 112, 044038, doi: [10.1103/jxrc-z298](https://doi.org/10.1103/jxrc-z298)
- Gerosa, D., & Bellotti, M. 2024, Quick recipes for gravitational-wave selection effects, Classical and Quantum Gravity, 41, 125002, doi: [10.1088/1361-6382/ad4509](https://doi.org/10.1088/1361-6382/ad4509)
- Gerosa, D., Mould, M., Gangardt, D., et al. 2021, A generalized precession parameter χ_p to interpret gravitational-wave data, Phys. Rev. D, 103, 064067, doi: [10.1103/PhysRevD.103.064067](https://doi.org/10.1103/PhysRevD.103.064067)
- Gerosa, D., Pratten, G., & Vecchio, A. 2020, Gravitational-wave selection effects using neural-network classifiers, Phys. Rev. D, 102, 103020, doi: [10.1103/PhysRevD.102.103020](https://doi.org/10.1103/PhysRevD.102.103020)
- Gommers, R., Virtanen, P., Haberland, M., et al. 2025, scipy/scipy: SciPy 1.16.2, v1.16.2 Zenodo, doi: [10.5281/zenodo.17101542](https://doi.org/10.5281/zenodo.17101542)
- Gondán, L., Kocsis, B., Raffai, P., & Frei, Z. 2018, Eccentric Black Hole Gravitational-wave Capture Sources in Galactic Nuclei: Distribution of Binary Parameters, ApJ, 860, 5, doi: [10.3847/1538-4357/aabfee](https://doi.org/10.3847/1538-4357/aabfee)
- Hamers, A. S., & Thompson, T. A. 2019, Double Neutron Star Mergers from Hierarchical Triple-star Systems, ApJ, 883, 23, doi: [10.3847/1538-4357/ab3b06](https://doi.org/10.3847/1538-4357/ab3b06)
- Hanna, C., Caudill, S., Messick, C., et al. 2020, Fast evaluation of multidetector consistency for real-time gravitational wave searches, Phys. Rev. D, 101, 022003, doi: [10.1103/PhysRevD.101.022003](https://doi.org/10.1103/PhysRevD.101.022003)
- Hanna, C., Kennington, J., Niu, W., et al. 2025, Template bank for subsolar mass compact binary mergers in the fourth observing run of Advanced LIGO, Advanced Virgo, and KAGRA, Phys. Rev. D, 112, 044013, doi: [10.1103/c97v-bmj8](https://doi.org/10.1103/c97v-bmj8)
- Harris, C. R., Millman, K. J., van der Walt, S. J., et al. 2020, Array programming with NumPy, Nature, 585, 357, doi: [10.1038/s41586-020-2649-2](https://doi.org/10.1038/s41586-020-2649-2)
- Harry, I., Bustillo, J. C., & Nitz, A. 2018, Searching for the full symphony of black hole binary mergers, Phys. Rev. D, 97, 023004, doi: [10.1103/PhysRevD.97.023004](https://doi.org/10.1103/PhysRevD.97.023004)
- Harry, I., Privitera, S., Bohé, A., & Buonanno, A. 2016, Searching for gravitational waves from compact binaries with precessing spins, Phys. Rev. D, 94, 024012, doi: [10.1103/PhysRevD.94.024012](https://doi.org/10.1103/PhysRevD.94.024012)
- Hunter, J. D. 2007, Matplotlib: A 2D graphics environment, Computing in Science & Engineering, 9, 90, doi: [10.1109/MCSE.2007.55](https://doi.org/10.1109/MCSE.2007.55)
- Isi, M., Chatziioannou, K., & Farr, W. M. 2019, Hierarchical Test of General Relativity with Gravitational Waves, Phys. Rev. Lett., 123, 121101, doi: [10.1103/PhysRevLett.123.121101](https://doi.org/10.1103/PhysRevLett.123.121101)
- Joshi, P., Tsukada, L., Hanna, C., et al. 2025a, New Methods for Offline GstLAL Analyses, arXiv e-prints, arXiv:2506.06497, doi: [10.48550/arXiv.2506.06497](https://doi.org/10.48550/arXiv.2506.06497)
- Joshi, P., Niu, W., Hanna, C., et al. 2025b, How Many Times Should We Matched Filter Gravitational Wave Data? A Comparison of GstLAL's Online and Offline Performance, arXiv e-prints, arXiv:2505.23959, doi: [10.48550/arXiv.2505.23959](https://doi.org/10.48550/arXiv.2505.23959)
- Kacanja, K., Soni, K., & Nitz, A. H. 2025, Eccentricity signatures in LIGO-Virgo-KAGRA's binary neutron star and neutron-star black holes, Phys. Rev. D, 112, 122007, doi: [10.1103/jnsc-783p](https://doi.org/10.1103/jnsc-783p)
- Kishore Roy, S., van Son, L. A. C., & Farr, W. M. 2025, A mid-thirties crisis: dissecting the properties of gravitational wave sources near the 35 solar mass peak, Classical and Quantum Gravity, 42, 225008, doi: [10.1088/1361-6382/ae1921](https://doi.org/10.1088/1361-6382/ae1921)
- Kluyver, T., Ragan-Kelley, B., Pérez, F., et al. 2016, Jupyter Notebooks – a publishing format for reproducible computational workflows, in Positioning and Power in Academic Publishing: Players, Agents and Agendas, ed. F. Loizides & B. Schmidt, IOS Press, 87 – 90
- Kramer, M., & Wex, N. 2009, TOPICAL REVIEW: The double pulsar system: a unique laboratory for gravity, Classical and Quantum Gravity, 26, 073001, doi: [10.1088/0264-9381/26/7/073001](https://doi.org/10.1088/0264-9381/26/7/073001)
- Kunnumkai, K., Palmese, A., O'Connor, B., Farah, A., & Magana Hernandez, I. 2026, Wide Jets or Low Rates: Reconciling Short GRB and Gravitational-Wave Neutron Star Merger Rates, arXiv e-prints, arXiv:2604.05046, doi: [10.48550/arXiv.2604.05046](https://doi.org/10.48550/arXiv.2604.05046)
- Leyde, K., Green, S. R., Dax, M., et al. 2026, End-to-End Population Inference from Gravitational-Wave Strain using Transformers, arXiv e-prints, arXiv:2605.11274, doi: [10.48550/arXiv.2605.11274](https://doi.org/10.48550/arXiv.2605.11274)
- LIGO Scientific Collaboration, Virgo Collaboration, & KAGRA Collaboration. 2018, LVK Algorithm Library - LALSuite, Free software (GPL) doi: [10.7935/GT1W-FZ16](https://doi.org/10.7935/GT1W-FZ16)
- LIGO Scientific Collaboration, Virgo Collaboration, & KAGRA Collaboration. 2023, GWTC-3: Compact Binary Coalescences Observed by LIGO and Virgo During the Second Part of the Third Observing Run — O1+O2+O3 Search Sensitivity Estimates, Zenodo, doi: [10.5281/zenodo.7890398](https://doi.org/10.5281/zenodo.7890398)
- LIGO Scientific Collaboration, Virgo Collaboration, & KAGRA Collaboration. 2025, GWTC-4.0 Cumulative Search Sensitivity Estimates, Zenodo, doi: [10.5281/zenodo.16740128](https://doi.org/10.5281/zenodo.16740128)
- LIGO Scientific Collaboration, Virgo Collaboration, & KAGRA Collaboration. 2026, Gravitational-Wave Candidate Event Database (GraceDB), <https://gracedb.ligo.org/>
- LIGO Scientific Collaboration, Aasi, J., Abbott, B. P., et al. 2015, Advanced LIGO, Classical and Quantum Gravity, 32, 074001, doi: [10.1088/0264-9381/32/7/074001](https://doi.org/10.1088/0264-9381/32/7/074001)
- Lorenzo-Medina, A., & Dent, T. 2025, A physically modelled selection function for compact binary mergers in the LIGO-Virgo O3 run and beyond, Classical and Quantum Gravity, 42, 045008, doi: [10.1088/1361-6382/ad9c0e](https://doi.org/10.1088/1361-6382/ad9c0e)
- Magee, R., Isi, M., Payne, E., et al. 2024, Impact of selection biases on tests of general relativity with gravitational-wave inspirals, Phys. Rev. D, 109, 023014, doi: [10.1103/PhysRevD.109.023014](https://doi.org/10.1103/PhysRevD.109.023014)
- Mehta, A. K., Wadekar, D., Roulet, J., et al. 2025, Significant increase in sensitive volume of a gravitational wave search upon including higher harmonics, arXiv e-prints, arXiv:2501.17939, doi: [10.48550/arXiv.2501.17939](https://doi.org/10.48550/arXiv.2501.17939)
- Messick, C., Blackburn, K., Brady, P., et al. 2017, Analysis framework for the prompt discovery of compact binary mergers in gravitational-wave data, Phys. Rev. D, 95, 042001, doi: [10.1103/PhysRevD.95.042001](https://doi.org/10.1103/PhysRevD.95.042001)
- Moore, B., Favata, M., Arun, K. G., & Mishra, C. K. 2016, Gravitational-wave phasing for low-eccentricity inspiralling compact binaries to 3PN order, Phys. Rev. D, 93, 124061, doi: [10.1103/PhysRevD.93.124061](https://doi.org/10.1103/PhysRevD.93.124061)

- Morras, G., Pratten, G., & Schmidt, P. 2025, Improved post-Newtonian waveform model for inspiralling precessing-eccentric compact binaries, *Phys. Rev. D*, 111, 084052, doi: [10.1103/PhysRevD.111.084052](https://doi.org/10.1103/PhysRevD.111.084052)
- Mould, M., Moore, C. J., & Gerosa, D. 2024, Calibrating signal-to-noise ratio detection thresholds using gravitational-wave catalogs, *Phys. Rev. D*, 109, 063013, doi: [10.1103/PhysRevD.109.063013](https://doi.org/10.1103/PhysRevD.109.063013)
- Mukherjee, D., Caudill, S., Magee, R., et al. 2021, Template bank for spinning compact binary mergers in the second observation run of Advanced LIGO and the first observation run of Advanced Virgo, *Phys. Rev. D*, 103, 084047, doi: [10.1103/PhysRevD.103.084047](https://doi.org/10.1103/PhysRevD.103.084047)
- Narola, H., Roy, S., & Sengupta, A. S. 2023, Beyond general relativity: Designing a template-based search for exotic gravitational wave signals, *Phys. Rev. D*, 107, 024017, doi: [10.1103/PhysRevD.107.024017](https://doi.org/10.1103/PhysRevD.107.024017)
- Nitz, A. H., Kumar, S., Wang, Y.-F., et al. 2023, 4-OGC: Catalog of Gravitational Waves from Compact Binary Mergers, *ApJ*, 946, 59, doi: [10.3847/1538-4357/aca591](https://doi.org/10.3847/1538-4357/aca591)
- Nitz, A. H., & Wang, Y.-F. 2021, Search for Gravitational Waves from the Coalescence of Subsolar Mass and Eccentric Compact Binaries, *ApJ*, 915, 54, doi: [10.3847/1538-4357/ac01d9](https://doi.org/10.3847/1538-4357/ac01d9)
- Owen, B. J. 1996, Search templates for gravitational waves from inspiraling binaries: Choice of template spacing, *Phys. Rev. D*, 53, 6749, doi: [10.1103/PhysRevD.53.6749](https://doi.org/10.1103/PhysRevD.53.6749)
- pandas development team, T. 2025, pandas-dev/pandas: Pandas, v2.3.3 Zenodo, doi: [10.5281/zenodo.17229934](https://doi.org/10.5281/zenodo.17229934)
- Perez, F., & Granger, B. E. 2007, IPython: A System for Interactive Scientific Computing, *Computing in Science and Engineering*, 9, 21, doi: [10.1109/MCSE.2007.53](https://doi.org/10.1109/MCSE.2007.53)
- Peters, P. C. 1964, Gravitational Radiation and the Motion of Two Point Masses, *Physical Review*, 136, 1224, doi: [10.1103/PhysRev.136.B1224](https://doi.org/10.1103/PhysRev.136.B1224)
- Phukon, K. S., Schmidt, P., Morras, G., & Pratten, G. 2026, Detection of GW200105 with a targeted eccentric search, *Phys. Rev. D*, 113, 103023, doi: [10.1103/cmtb-5q4b](https://doi.org/10.1103/cmtb-5q4b)
- Planas, M. d. L., Ramos-Buades, A., García-Quirós, C., et al. 2026, Time-domain phenomenological multipolar waveforms for aligned-spin binary black holes in elliptical orbits, *Phys. Rev. D*, 113, 024006, doi: [10.1103/wz3v-b151](https://doi.org/10.1103/wz3v-b151)
- Pratten, G., García-Quirós, C., Colleoni, M., et al. 2021, Computationally efficient models for the dominant and subdominant harmonic modes of precessing binary black holes, *Phys. Rev. D*, 103, 104056, doi: [10.1103/PhysRevD.103.104056](https://doi.org/10.1103/PhysRevD.103.104056)
- Ramos-Buades, A., Henry, Q., & Haney, M. 2026, Fast frequency-domain phenomenological modeling of eccentric aligned-spin binary black holes, *Phys. Rev. D*, 113, 083044, doi: [10.1103/5bcn-k5s6](https://doi.org/10.1103/5bcn-k5s6)
- Ray, A., Niu, W., Sakon, S., et al. 2023, When to Point Your Telescopes: Gravitational Wave Trigger Classification for Real-Time Multi-Messenger Followup Observations, arXiv e-prints, arXiv:2306.07190, doi: [10.48550/arXiv.2306.07190](https://doi.org/10.48550/arXiv.2306.07190)
- Rodriguez, C. L., Amaro-Seoane, P., Chatterjee, S., & Rasio, F. A. 2018, Post-Newtonian Dynamics in Dense Star Clusters: Highly Eccentric, Highly Spinning, and Repeated Binary Black Hole Mergers, *Phys. Rev. Lett.*, 120, 151101, doi: [10.1103/PhysRevLett.120.151101](https://doi.org/10.1103/PhysRevLett.120.151101)
- Roy, S., Sengupta, A. S., & Ajith, P. 2017a, Effectual gravitational-wave template banks for coalescing compact binaries using a hybrid placement algorithm, arXiv e-prints, arXiv:1711.08743, doi: [10.48550/arXiv.1711.08743](https://doi.org/10.48550/arXiv.1711.08743)
- Roy, S., Sengupta, A. S., & Thakor, N. 2017b, Hybrid geometric-random template-placement algorithm for gravitational wave searches from compact binary coalescences, *Phys. Rev. D*, 95, 104045, doi: [10.1103/PhysRevD.95.104045](https://doi.org/10.1103/PhysRevD.95.104045)
- Roy, S., & Vicente, R. 2025, Compact binary coalescences in dense gaseous environments can pose as ones in vacuum, *Phys. Rev. D*, 111, 084037, doi: [10.1103/PhysRevD.111.084037](https://doi.org/10.1103/PhysRevD.111.084037)
- Sakon, S., Tsukada, L., Fong, H., et al. 2024, Template bank for compact binary mergers in the fourth observing run of Advanced LIGO, Advanced Virgo, and KAGRA, *Phys. Rev. D*, 109, 044066, doi: [10.1103/PhysRevD.109.044066](https://doi.org/10.1103/PhysRevD.109.044066)
- Samsing, J., Bartos, I., D’Orazio, D. J., et al. 2022, AGN as potential factories for eccentric black hole mergers, *Nature*, 603, 237, doi: [10.1038/s41586-021-04333-1](https://doi.org/10.1038/s41586-021-04333-1)
- Shariat, C. 2026, OverCite: Add Citations in LaTeX without Leaving the Editor, *Research Notes of the American Astronomical Society*, 10, 86, doi: [10.3847/2515-5172/ae5dbc](https://doi.org/10.3847/2515-5172/ae5dbc)
- Sharma, A., Roy, S., & Sengupta, A. S. 2024, Template bank to search for exotic gravitational wave signals from astrophysical compact binaries, *Phys. Rev. D*, 109, 124049, doi: [10.1103/PhysRevD.109.124049](https://doi.org/10.1103/PhysRevD.109.124049)
- Silsbee, K., & Tremaine, S. 2017, Lidov-Kozai Cycles with Gravitational Radiation: Merging Black Holes in Isolated Triple Systems, *ApJ*, 836, 39, doi: [10.3847/1538-4357/aa5729](https://doi.org/10.3847/1538-4357/aa5729)
- Talbot, C., & Thrane, E. 2020, Fast, flexible, and accurate evaluation of gravitational-wave Malmquist bias with machine learning, arXiv e-prints, arXiv:2012.01317, doi: [10.48550/arXiv.2012.01317](https://doi.org/10.48550/arXiv.2012.01317)
- The LIGO Scientific Collaboration, the Virgo Collaboration, & the KAGRA Collaboration. 2026a, GWTC-5.0: Methods for Identifying and Characterizing Gravitational-wave Transients, arXiv e-prints, arXiv:2605.27224, doi: [10.48550/arXiv.2605.27224](https://doi.org/10.48550/arXiv.2605.27224)
- The LIGO Scientific Collaboration, the Virgo Collaboration, & the KAGRA Collaboration. 2026b, GWTC-5.0: Observations from the Second Part of the Fourth LIGO-Virgo-KAGRA Observing Run and Updates to the Gravitational-Wave Transient Catalog, arXiv e-prints, arXiv:2605.27225, doi: [10.48550/arXiv.2605.27225](https://doi.org/10.48550/arXiv.2605.27225)
- The LIGO Scientific Collaboration, the Virgo Collaboration, the KAGRA Collaboration, et al. 2025a, GWTC-4.0: Updating the Gravitational-Wave Transient Catalog with Observations from the First Part of the Fourth LIGO-Virgo-KAGRA Observing Run, arXiv e-prints, arXiv:2508.18082, doi: [10.48550/arXiv.2508.18082](https://doi.org/10.48550/arXiv.2508.18082)
- The LIGO Scientific Collaboration, the Virgo Collaboration, the KAGRA Collaboration, et al. 2025b, GWTC-4.0: Population Properties of Merging Compact Binaries, arXiv e-prints, arXiv:2508.18083, doi: [10.48550/arXiv.2508.18083](https://doi.org/10.48550/arXiv.2508.18083)
- The LIGO Scientific Collaboration, the Virgo Collaboration, the KAGRA Collaboration, et al. 2026c, GWTC-4.0: Tests of General Relativity. II. Parameterized Tests, arXiv e-prints, arXiv:2603.19020, doi: [10.48550/arXiv.2603.19020](https://doi.org/10.48550/arXiv.2603.19020)
- Tiwari, A., Vijaykumar, A., Kapadia, S. J., Chatterjee, S., & Fragione, G. 2025, Profiling stellar environments of gravitational wave sources, *Phys. Rev. D*, 112, 084034, doi: [10.1103/gspl-m478](https://doi.org/10.1103/gspl-m478)
- Tsukada, L., Joshi, P., Adhichary, S., et al. 2023, Improved ranking statistics of the GstLAL inspiral search for compact binary coalescences, *Phys. Rev. D*, 108, 043004, doi: [10.1103/PhysRevD.108.043004](https://doi.org/10.1103/PhysRevD.108.043004)
- Van Rossum, G., & Drake, F. L. 2009, *Python 3 Reference Manual* (Scotts Valley, CA: CreateSpace)
- Vijaykumar, A., Hanselman, A. G., & Zevin, M. 2024, Consistent Eccentricities for Gravitational-wave Astronomy: Resolving Discrepancies between Astrophysical Simulations and Waveform Models, *ApJ*, 969, 132, doi: [10.3847/1538-4357/ad4455](https://doi.org/10.3847/1538-4357/ad4455)
- Vijaykumar, A., Tiwari, A., Kapadia, S. J., Arun, K. G., & Ajith, P. 2023, Waltzing Binaries: Probing the Line-of-sight Acceleration of Merging Compact Objects with Gravitational Waves, *ApJ*, 954, 105, doi: [10.3847/1538-4357/acd77d](https://doi.org/10.3847/1538-4357/acd77d)
- Virtanen, P., Gommers, R., Oliphant, T. E., et al. 2020, *SciPy 1.0: Fundamental Algorithms for Scientific Computing in Python*, *Nature Methods*, 17, 261, doi: [10.1038/s41592-019-0686-2](https://doi.org/10.1038/s41592-019-0686-2)
- Wadekar, D., Venumadhav, T., Roulet, J., et al. 2024, New search pipeline for gravitational waves with higher-order modes using mode-by-mode filtering, *Phys. Rev. D*, 110, 044063, doi: [10.1103/PhysRevD.110.044063](https://doi.org/10.1103/PhysRevD.110.044063)
- Wagg, T., Broekgaarden, F., & Gültekin, K. 2025, TomWagg/software-citation-station: v1.3, v1.3 Zenodo, doi: [10.5281/zenodo.17145205](https://doi.org/10.5281/zenodo.17145205)
- Wagg, T., & Broekgaarden, F. S. 2024, Streamlining and standardizing software citations with The Software Citation Station, arXiv e-prints, arXiv:2406.04405, <https://arxiv.org/abs/2406.04405>
- Waskom, M. L. 2021, seaborn: statistical data visualization, *Journal of Open Source Software*, 6, 3021, doi: [10.21105/joss.03021](https://doi.org/10.21105/joss.03021)
- Wen, L. 2003, On the Eccentricity Distribution of Coalescing Black Hole Binaries Driven by the Kozai Mechanism in Globular Clusters, *ApJ*, 598, 419, doi: [10.1086/378794](https://doi.org/10.1086/378794)
- Wes McKinney. 2010, *Data Structures for Statistical Computing in Python*, in *Proceedings of the 9th Python in Science Conference*, ed. Stefan van der Walt & Jarrod Millman, 56 – 61, doi: [10.25080/Majora-92bf1922-00a](https://doi.org/10.25080/Majora-92bf1922-00a)
- Wette, K. 2020, SWIGLAL: Python and Octave interfaces to the LALSuite gravitational-wave data analysis libraries, *SoftwareX*, 12, 100634, doi: [10.1016/j.softx.2020.100634](https://doi.org/10.1016/j.softx.2020.100634)
- Wysocki, D., Lange, J., & O’Shaughnessy, R. 2019, Reconstructing phenomenological distributions of compact binaries via gravitational wave observations, *Phys. Rev. D*, 100, 043012, doi: [10.1103/PhysRevD.100.043012](https://doi.org/10.1103/PhysRevD.100.043012)
- Yang, Y., Bartos, I., Gayathri, V., et al. 2019, Hierarchical Black Hole Mergers in Active Galactic Nuclei, *Phys. Rev. Lett.*, 123, 181101, doi: [10.1103/PhysRevLett.123.181101](https://doi.org/10.1103/PhysRevLett.123.181101)
- Zevin, M., Romero-Shaw, I. M., Kremer, K., Thrane, E., & Lasky, P. D. 2021, Implications of Eccentric Observations on Binary Black Hole Formation Channels, *ApJ*, 921, L43, doi: [10.3847/2041-8213/ac32dc](https://doi.org/10.3847/2041-8213/ac32dc)

provides fast and easy peer review for new papers in the **astro-ph** section of the arXiv, making the reviewing pro-

cess simpler for authors and referees alike. Learn more at <http://astro.theoj.org>.